

## High power laser interaction with single and double layer targets

STEFAN BORODZIUK<sup>1</sup>, NIKOLAY N. DEMCHENKO<sup>2</sup>, SERGEY YU. GUS'KOV<sup>2</sup>, KAREL JUNGWIRTH<sup>3</sup>, MILAN KALAL<sup>4</sup>, ANDRZEJ KASPERCZUK<sup>1</sup>, VLADIMIR N. KONDRASHOV<sup>5</sup>, BOZENA KRALIKOVA<sup>3</sup>, EDWARD KROUSKY<sup>3</sup>, JIRI LIMPOUCH<sup>3,4</sup>, KAREL MASEK<sup>3</sup>, PAWEL PISARCZYK<sup>6</sup>, TADEUSZ PISARCZYK<sup>1</sup>, MIROSLAV PFEIFER<sup>3</sup>, KAREL ROHLENA<sup>3</sup>, VLADISLAV B. ROZANOV<sup>3</sup>, JIRI SKALA<sup>3</sup>, JIRI ULLSCHMIED<sup>3</sup>

<sup>1</sup>Institute of Plasma Physics and Laser Microfusion, Hery 23, 00-908 Warszawa, Poland

<sup>2</sup>P.N. Lebedev Physical Institute of RAS, Leninsky 53, 119 991 Moscow, Russia

<sup>3</sup>PALS Research Center, AS CR, Na Slovance 3, 182 21 Prague 8, Czech Republic

<sup>4</sup>Czech Technical University in Prague, FNSPE, Brehova 7, 115 19 Prague 1, Czech Republic

<sup>5</sup>Troitsk Institute of Innovation and Thermonuclear Research, 142 190 Troitsk, Russia

<sup>6</sup>Warsaw University of Technology, ICS, Nowowiejska 15/19, 00-665 Warszawa, Poland

Results of extended complementary experimental and computer simulation studies of craters formation produced by high power lasers in single and double layer targets are presented. The experimental investigation was carried out using the PALS (Prague Asterix Laser System) facility working with two different laser beam wavelengths:  $\lambda_1 = 1.315 \mu\text{m}$  and  $\lambda_3 = 0.438 \mu\text{m}$ . Two types of targets made of Al were used: single massive targets and double targets consisting of foils or disks (6 and 11  $\mu\text{m}$  thick for both cases) placed in front of the massive target at distances of 200 and 500  $\mu\text{m}$ . The targets were illuminated by laser energies  $E_L = 130, 240$  and 390 J always focused with diameter of 250  $\mu\text{m}$ . In all experiments performed the laser pulse duration was equal to 400 ps. The 3-frame interferometry was employed to investigate the plasma dynamics by means of the electron density distribution time development, as well as the disks and foil fragments velocity measurements. Dimensions and shapes of craters were obtained by crater replica technology and microscopy measurement. Experimental results were complemented by analytical theory and computer simulations to help their interpretation. This way the values of laser energy absorption coefficient, ablation loading efficiency and efficiency of energy transfer, as well as 2-D shock wave generation at the laser-driven macroparticle impact, were obtained from measured craters parameters for both wavelengths of laser radiation. Computer simulations allowed us to obtain an energy absorption balance of incident laser energy for both wavelengths employed.

Keywords: laser produced plasma, three-frame interferometry, macroparticle, single and double targets, crater, shock wave, laser energy absorption.

## 1. Introduction

Success of laser-driven fusion depends on the ablative compression of spherical targets. Construction of a more powerful laser system and the development of better target designs approach the problem of high efficiency of inertial confinement fusion (ICF). Because of the complex nature of phenomena accompanying the laser–target interaction (*e.g.*, laser pulse uniformity requirements, absorption efficiency of laser radiation and mechanism of radiation absorption) and plasma ablation (ablation pressure and shock wave generation, heat transport, energy transfer into shock wave and fast electrons, Rayleigh–Taylor instability and so on), *e.g.*, [1–5] there is still free space for experiments studying above mentioned physical aspects.

The experiments utilizing ablatively accelerated planar targets can model large pellet shells in their early implosion phase. Instead of imploding a pellet, a disk made of thin foil can be accelerated and treated as a section of sphere (as long as convergence effect dominate). When thin foil accelerated by means of a laser beam to reach a velocity of more than  $10^7$  cm/s collides with a target at rest, a very strong shock wave and pressure of order of 100 Mbar can be generated.

The main aims of our investigations were to determine the macroparticle acceleration and crater creation efficiency in dependence on: i) the origin of a macroparticle (extracted foil or disk), ii) the wavelength of a laser beam. In the first case, we supposed that, contrary to the foil variant, the disk could be accelerated with negligible energy loss required on its extraction and no lateral heat conduction loss. The second aim was connected with different absorption of laser beam energy for the first and the third harmonic. In terms of theoretical prediction, the shorter wavelength ought to be more effective.

To realize the above goals, two types of planar aluminium targets were used: the single massive target and several variants of the so-called double (or flyer plate) targets, particularly prepared for this experiment. Special attention was paid to craters produced in the massive target. Perhaps, they constitute the most evident results of the laser–massive target experiment and, simultaneously, are a very convenient source of useful data for better comprehension of many features of interest.

To study the temporal behaviour of the plasma expansion of the irradiated target (single or double) as well as the ablatively accelerated thin foil or disk (in the case of the double targets) a three-frame interferometric system was used. Additionally, a crater replica technology and an optical microscopy were applied to measure the crater dimensions (depth and diameter) and to determine shapes of craters produced in the massive targets.

These measurements were complemented by suitable theoretical models and computer simulations (in which two-dimensional hydrodynamic numerical code was applied) to provide information about the plasma parameters and physics involved (laser radiation absorption efficiency, hydrodynamic efficiency of the energy transfer to the shock wave propagating in the massive target, thermal conductivity and so on) [6].

## 2. Experimental set-up and diagnostics

### 2.1. Experimental conditions

Experimental investigations of the crater formation process by means of a double-target technique were performed on the PALS iodine laser facility [7]. Its view is presented in Fig. 1.

The detailed optical scheme of the PALS facility is shown in Fig. 2. Investigations were carried out employing two harmonics of laser radiation:  $\lambda_1 = 1.315 \mu\text{m}$  and  $\lambda_3 = 0.438 \mu\text{m}$ .

In these experiments several different types of targets were used: single massive planar Al targets as well as much more elaborated double targets consisting of Al foils or disks placed in front of the massive target. The experimental conditions were varied by changing the foil thickness, laser focal spot diameter, laser intensity, and the distance between the irradiated foil and the massive target.



Fig. 1. View of the PALS iodine laser facility.

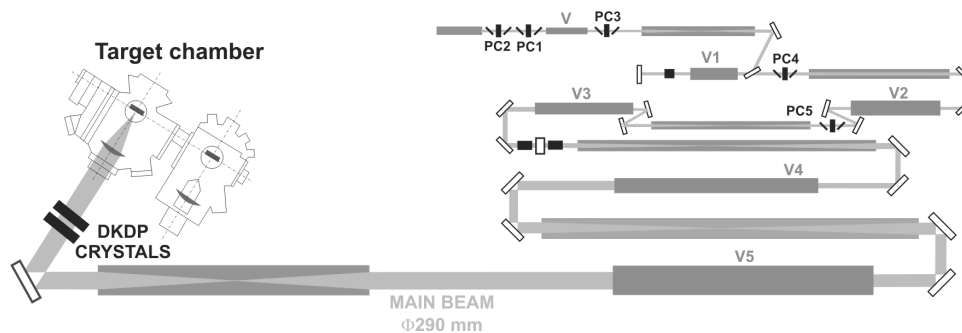


Fig. 2. Optical scheme of the PALS facility (OSC – mode-locked oscillator, PC – Pockels cell, V – amplifiers, RF – space filters).

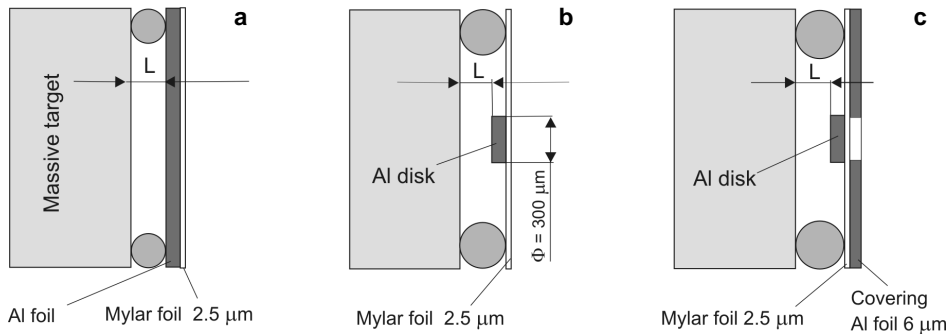


Fig. 3. Constructions of the double targets: **a** – foil and massive target, **b** – disk and massive target, and **c** – shielded disk and massive target.

The following conditions of target irradiation were applied:

- first harmonic for laser energies  $E_L = 130, 240$  and  $390$  J,
- third harmonic for laser energy  $E_L = 130$  J,
- laser pulse duration  $\tau = 400$  ps,
- focal spot radius  $R_L = 125$   $\mu\text{m}$ .

In the experiments the double targets consisting of foils or disks (6 or 11  $\mu\text{m}$  thick) and placed before a slab at distances  $L = 200$  and  $500$   $\mu\text{m}$  were employed. Double targets with the gap of  $500$   $\mu\text{m}$  were used for the accelerated macroparticle velocity determination (this gap was large enough for registration of two subsequent frames during the macroparticle flight). However, from the point of view of the crater creation itself, such a long distance seemed to be rather unprofitable due to a possibility of accelerated (and heated) macroparticle premature disintegration. Thus for this purpose the shorter distance of  $200$   $\mu\text{m}$  was constituted. The constructions of the used double targets are presented in Fig. 3. Disks were attached to a supporting  $2.5$   $\mu\text{m}$  thick mylar foil on the side opposite to the incoming laser beam. To keep the same conditions of the target heating as in the disk case, the front side of the all remaining double targets was also covered by the same mylar foil.

## 2.2. Interferometry

To study the plasma expansion and macroparticle acceleration, a 3-frame interferometric system with automatic data acquisition and image processing was used [8]. The optical scheme of this system (illuminated by the third harmonic of the iodine laser  $\lambda_3 = 438$  nm) is presented in Fig. 4.

Each of the interferometric channels is equipped with its own independent interferometer of the folding wave type [9, 10]. The diagnostic beam used for target illumination was obtained as a part of the main laser beam subsequently converted to the third harmonic. Basic principle of operation of these individual interferometers is presented in Fig. 5.

Interferograms provided by these interferometers are obtained by separation, inversion, and folding of the front face of the probing wave. According to the principle

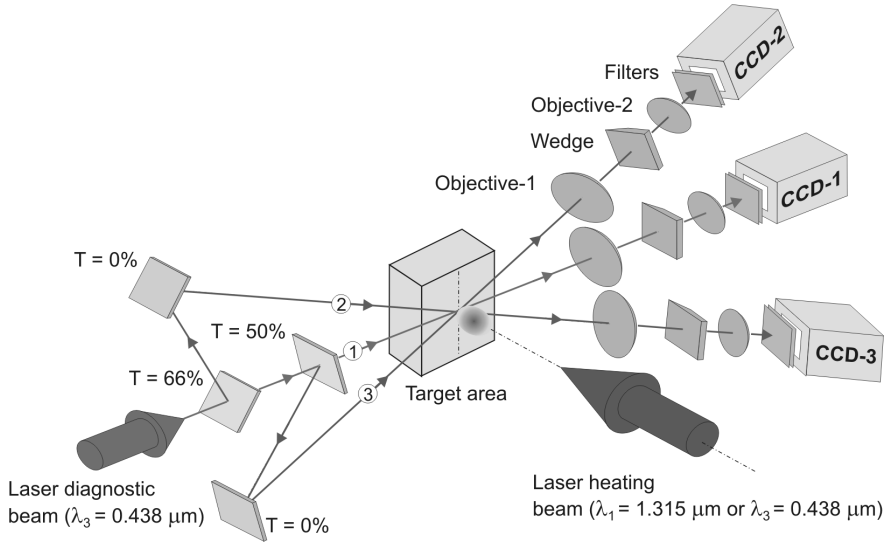


Fig. 4. 3-frame interferometric system.

of operation of this interferometer the diameter of the probing beam should be at least twice as large as the investigated plasma dimension. From analysis of the optical scheme of the interferometer one can derive the following formulas for describing the width of interference fringe  $\Delta d$ , and the distance between the object beam and the reference beam in the registration plane  $d$  [10]:

$$\Delta d = \frac{(b - f)\lambda}{2nf\gamma}, \tag{1}$$

$$d = \frac{1}{2} \left[ b - \left( \frac{b}{f} - 1 \right) l \right] n\gamma \tag{2}$$

where:  $\gamma$  – wedge refraction angle,  $\lambda$  – probing radiation wavelength,  $n$  – wedge refractive index,  $f$  – objective focal length.

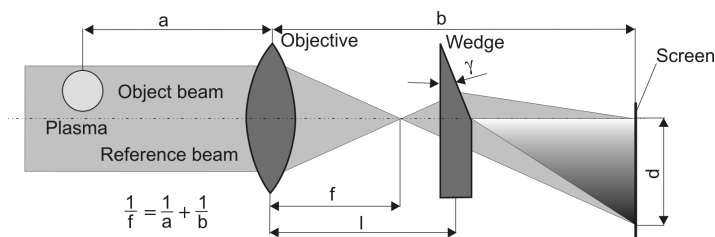


Fig. 5. Principle of operation of individual interferometers.



Fig. 6. View of the plasma chamber and interferometric registration system.

Using the above formulas the optimal conditions of the registration were determined. The interferometric measurements (which are presented in this paper) were carried out with the objective focal length  $f = 250$  mm, the angle of the wedge  $\gamma = 3^\circ$  and the enlargement of approximately five times. This arrangement made it possible to obtain the required separation of the interferometric fringes close to  $40 \mu\text{m}$  in the registration plane of the interferogram.

Each of the recording interferometric channels was equipped with one CCD camera of the Pulnix TM-1300 type, with the matrix of  $1300 \times 1030$  pixels.

As the delay between subsequent frames was set to 3 ns the interferometric measurement during a single shot could cover a period of 6 ns, enough for the observation of macroparticles acceleration. Delays of frames are related to the maximum of the heating laser pulse (0 ns). The vacuum chamber and the 3-frame interferometric set-up are shown in Fig. 6.

Typical sequences of interferograms obtained by means of the 3-frame interferometer, showing the ablative plasma expansion as well as the foil (**a**) and disk (**b**) motion in the case of the first harmonic, are presented in Fig. 7.

On the basis of interferometric measurements it was possible to determine the axial velocity of the acceleration foil and disk as well as electron density distribution of the ablative plasma. In the case of axial symmetry of the plasma, the relation between the phase of the probing radiation and the electron plasma density in a selected cross section (at the distance  $z$ ) can be expressed by the well known Abel integral formula:

$$S(y) = 2 \int_y^1 \frac{f(r)r}{\sqrt{r^2 - y^2}} dr \quad (3)$$

where  $f(r) = 4.46 \times 10^{-14} \lambda R n_e(r)$ ,  $y$  and  $r$  – the corresponding coordinates in the interference plane and in the real plasma cross-section, respectively [cm],  $S(y)$  – the

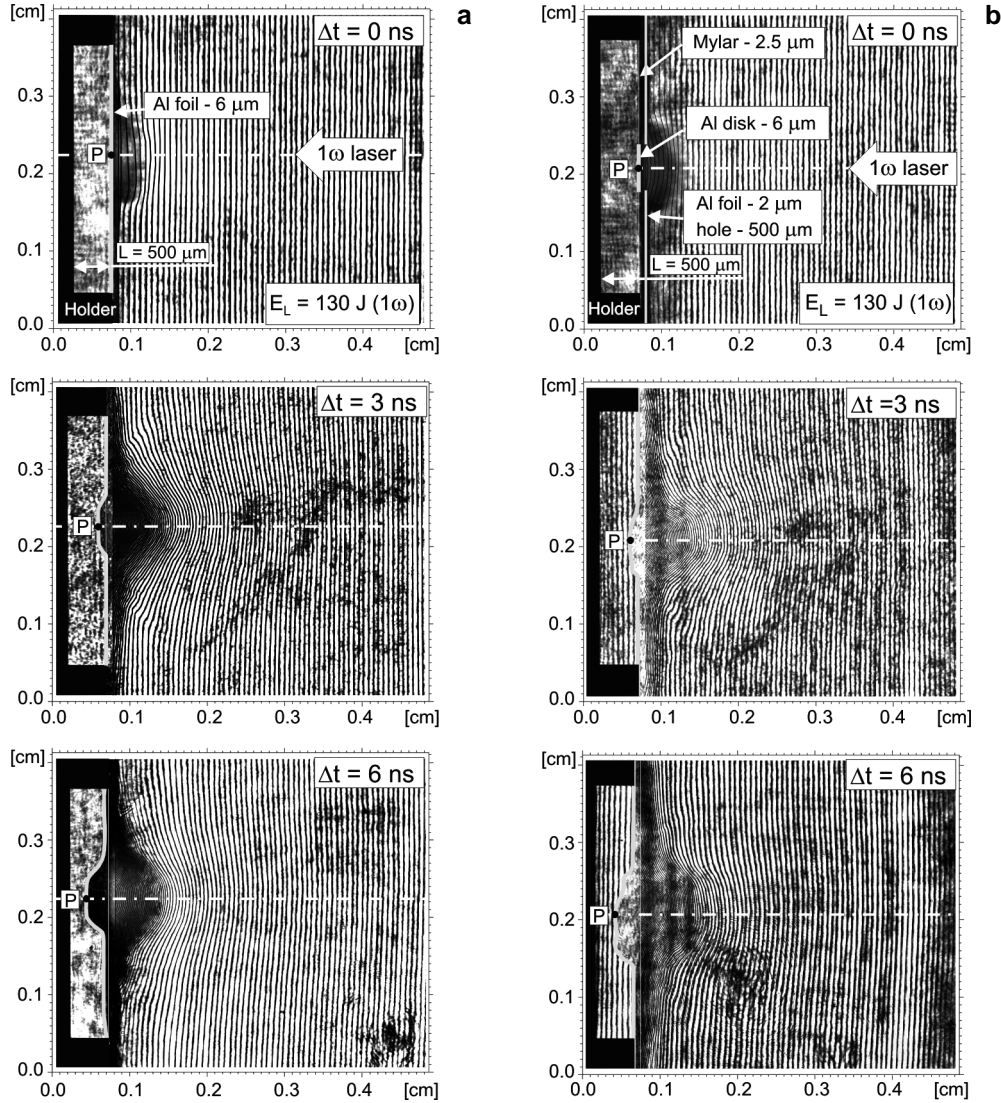


Fig. 7. Sequences of interferograms illustrating the ablative plasma expansion as well as foil (a) and disk (b) acceleration.

phase distribution  $[\text{rad}/2\pi]$ ,  $n_e(r)$  – the electron density distribution  $[\text{cm}^{-3}]$ ,  $\lambda$  – the laser radiation wavelength  $[\text{cm}]$ ,  $R$  – the plasma radius of the cross-section  $[\text{cm}]$ .

To determine the electron density distribution on the basis of the phase shift, the special numerical methods have been developed [8, 11]. Calculation of the  $n_e(r)$  distributions in many cross-sections along the  $z$ -axis allows for the reconstruction of the full plasma electron density distribution  $n_e(r, z)$  which can be presented in various graphical forms.

### 2.3. Optical microscopy

Information about the efficiency of the laser target interaction is accessible from the crater parameters, *i.e.*, their shape and dimensions. On the basis of the craters volume measurements the efficiency  $\beta$  of the energy transfer from the fast macroparticle to the massive target may be found by the formula:

$$\beta = \frac{V_{c(\text{double})}}{V_{c(\text{single})}} \quad (4)$$

where  $V_{c(\text{double})}$  and  $V_{c(\text{single})}$  are the double and single target crater volumes, respectively.

In order to obtain information about the shape and dimensions of the craters, their replicas were made of acetate cellulose. To reconstruct quantitatively the crater shape, the crater replica microphotography was employed. Then the crater shape in a chosen cross-section was digitized to provide data for subsequent calculations.

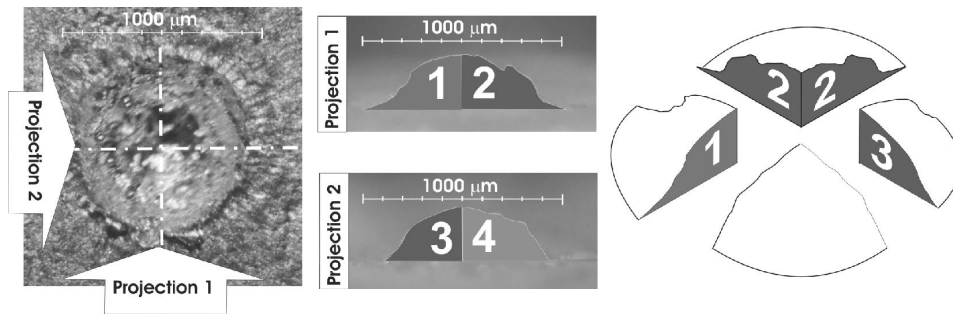


Fig. 8. Crater volume determination.

As some craters are not quite symmetrical and their shapes are irregular, their replica photographs were obtained in two mutually perpendicular directions. Due to this fact the volumes of the craters were determined on the basis of splitting them at first into quarters (Fig. 8). Each quarter of the crater volume was then determined independently. Finally, summation of these intermediate results provided the total crater volume.

## 3. Results of experimental investigations and discussion

### 3.1. Crater formation by 1st harmonic of laser radiation

The fundamental investigations of crater formation process by means of the double-target technique using the first harmonic of laser irradiation were performed. Targets were irradiated by the PALS iodine laser beam:  $E_L = 130, 240$  and  $390$  J, the focal spot radius of  $125 \mu\text{m}$ , and the pulse duration of  $400$  ps.

T a b l e 1. Set of average macroparticle velocities.

Laser energy	Foil fragment velocity	Disk velocity
130 J	$3.4 \times 10^6$ cm/s	$4.0 \times 10^6$ cm/s
240 J	$4.8 \times 10^6$ cm/s	$5.4 \times 10^6$ cm/s

In these experiments the single Al massive target and two types of double targets were selected and applied [12–14]: i) the first target type with a thickness of the foil and/or disk of 11  $\mu\text{m}$  placed at the distance of 500  $\mu\text{m}$  from the massive target (optimal from the point of view of accelerated foil fragments and/or disks velocity measurement), ii) the second target type with the same thickness of the foil and/or the disk as above, but with the distance of 200  $\mu\text{m}$  (optimal for the actual crater creation). Constructions of these double targets were shown earlier in Fig. 3. This way the measurements of axial velocity of the accelerated foil and/or disk for laser energies up to 300 J were possible. For the laser energies above 300 J the X-ray radiation intensity was already so strong that after its penetration through the heated foil it started to generate rather dense plasma from the massive target surface itself. This plasma strongly hindered the observation of the motion of macroparticles. Therefore, it was possible to determine the average velocities of the foil fragments and the disks only for the two lowest laser energies applied (130 and 240 J). Their respective values are presented in Tab. 1.

These results clearly demonstrate that the velocities of the accelerated disks are by 10–15% higher when compared with the velocities of the accelerated foil fragments.

Typical shapes of the craters for the targets tested at three different laser energies (130, 240, and 390 J) are presented in Fig. 9. From these shapes the following conclusions could be formulated:

- The craters obtained as a result of the direct laser beam-massive target interaction have approximately hemispherical shapes for all the laser energies applied;
- For the double targets consisting of the foil and the massive plate, the craters acquire completely different shapes when compared to the previous case. Here the craters are relatively shallow but their diameters appear to be slightly bigger. The shapes of the craters are still reasonably symmetrical;
- The craters created by the disks strongly depend on the laser energy. For the lowest laser energy of 130 J, the crater shape is similar to that obtained by the direct laser action. With the laser energy increase, the crater shapes become more and more irregular.

The volumes of the craters shown in Fig. 9 are presented in Fig. 10 in the form of diagrams. These diagrams show some tendencies in the craters volume changes as a function of the laser energy within the laser energy range employed. In the case of the massive target alone as well as for the combination of the foil and the massive target the crater volume grows linearly with laser energy (even though in the first case the crater volumes are much larger). In the disk case the crater volume increase is stopped for laser energies above 250 J.

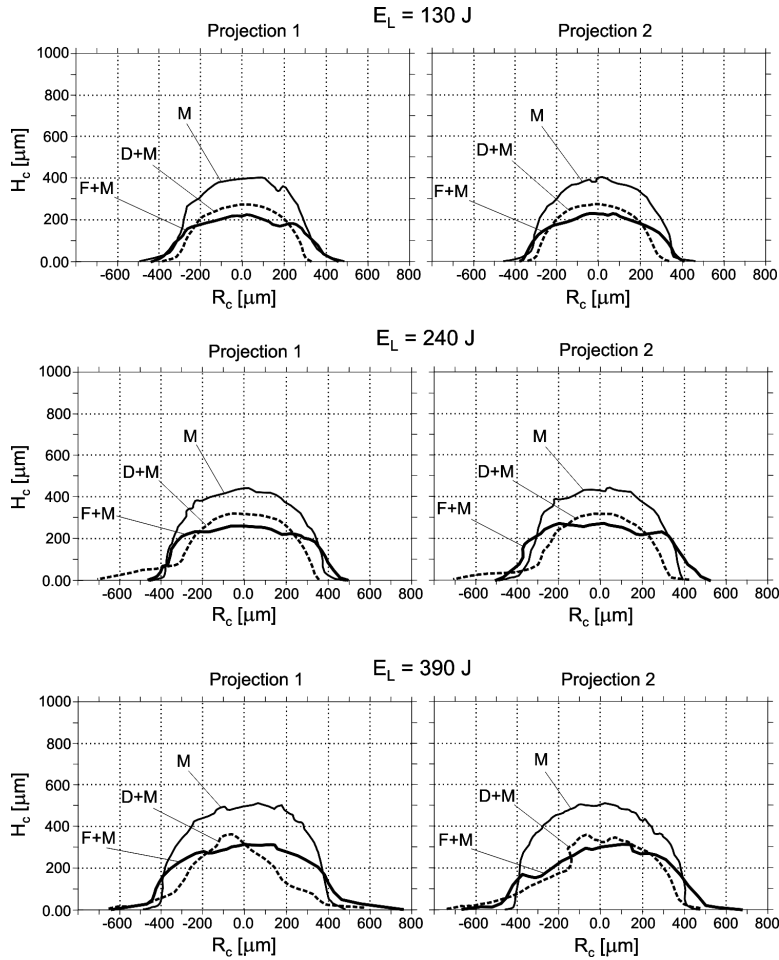


Fig. 9. Illustration of the crater shapes and dimensions for the tested targets and for three different values of the laser energy applied. Notations: M – massive target, F+M – double target with foil, and D+M – double target with disk.

By application of the formula (4) to the experimental data from Fig. 10 the efficiency  $\beta$  of the energy transfer from the foil or the disk to the massive target was established. In the energy range of 130–240 J the average values of  $\beta$  amount to 0.75 and 0.6 for the foil and the disk, respectively.

### 3.1.1. Conclusions from $1\omega$ experiments

The above investigations clearly confirm that the direct action of the laser beam on the massive target is the most efficient way of crater creation. Such craters have approximately hemispherical shapes (at least in the case of the wavelength used in our experiments with  $\lambda_1 = 1.315 \mu\text{m}$ ) and their volume linearly grows with the laser beam energy.

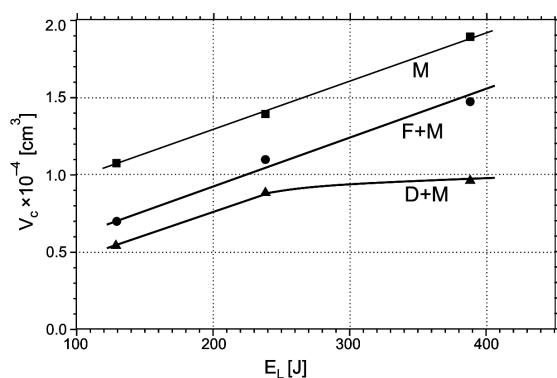


Fig. 10. Diagrams of the crater volumes as a function of the laser energy for different types of targets. Notations are the same as in Fig. 9.

The crater generation method by means of ablatively accelerated thin foil fragments colliding with a massive target is less effective. Transfer of the laser energy into the massive target via the foil fragment cannot, obviously, be as efficient as the direct massive target illumination. In terms of the diagrams from Fig. 10 it could be concluded that in this indirect case of crater generation the efficiency grows with the laser energy increase.

This indirect method, however, exhibits some useful features, as by changing the foil thickness, laser focal spot diameter (determining the extracted foil fragment diameter), laser energy, and the distance between the irradiated foil and the massive target, it is possible to obtain a wide range of macroparticle velocities and diameters for experimentation.

The results concerning the velocities of the accelerated disks are not unexpected, as these velocities are indeed higher than those for the extracted foil fragments. However, the craters obtained by means of the latter method are not only noticeably smaller but also the initially linear growth of their volumes with the increase in the laser energy applied is suppressed above a certain energy level (with crater shapes irregularities becoming rather typical of such above-threshold energies).

The regular shapes of the craters produced at the lowest laser energy applied (130 J) prove beyond any doubt that the disks can keep their original form reasonably well even after their extraction from the mylar support. However, even if the disks move with a slightly higher velocity in comparison with the velocity of the foil fragments, the crater volumes created by the foil fragments are larger. For higher laser energies the efficiency of the crater creation by the disks is further decreasing.

These results may be explained by physical processes of the energy transfer from the laser beam to the target, taking into account two-dimensional plasma expansion of the evaporated target part. The laser-driven loading efficiencies (defined as the ratio of the shock wave energy to the laser energy) for a single massive target and for a double target with a thick foil (when the foil thickness is larger than the depth the shock wave penetrates during the laser pulse action) are close to each other. Thus the smaller

crater volume in the case of this type of a double target is associated only with the efficiency of the energy transfer from the macroparticle to the massive target during the impact. This efficiency is approximately equal to 75%. The smaller volume of the crater in the case of the double target with the disk, when compared to that created by the foil fragment, can be explained by lower efficiency of the laser energy absorption to the solid part of the disk. This decrease in the loading efficiency becomes more pronounced with the increasing laser energy and it results from the two-dimensional expansion of the plasma torch. As a result, the radius of the area of the evaporated material pressure action exceeds the disk radius. Thus, for any fixed disk radius, a degree of this excess grows with the laser energy increase, as the speed of the target material evaporation grows simultaneously with such laser energy increase as well.

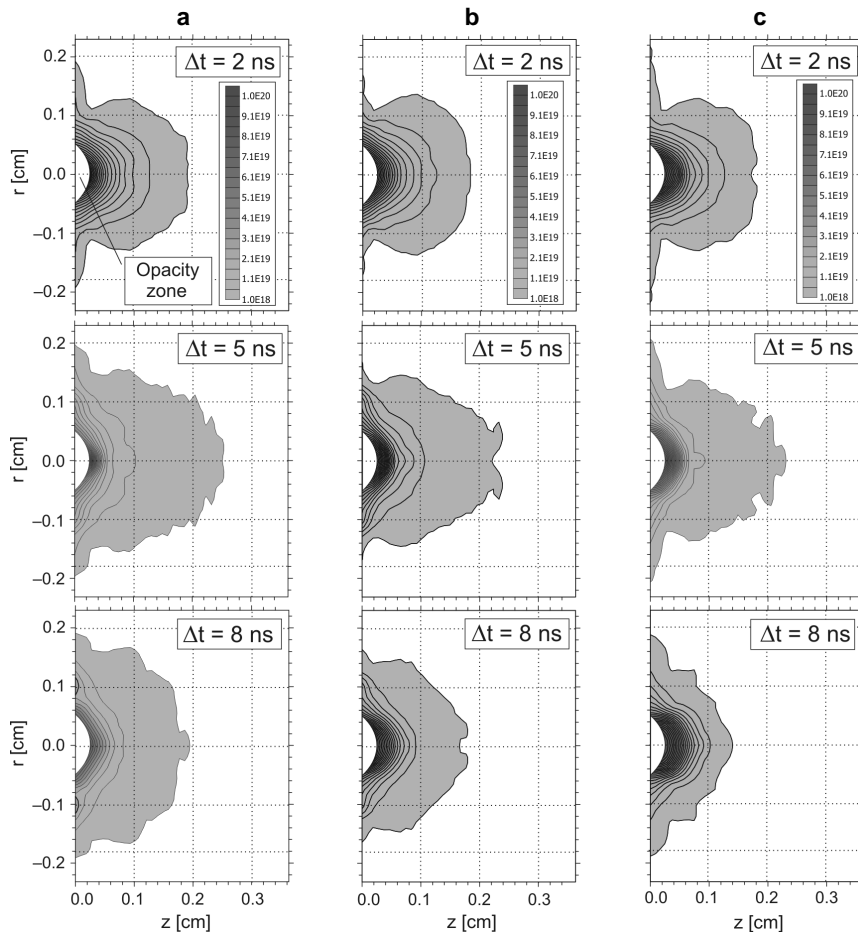


Fig. 11. Sequences of the electron density isodensitograms for the first harmonic of the laser radiation and the three types of targets: **a** – single massive target, **b** – double target with foil, and **c** – double target with disk.

More detailed analysis [12] showed that the laser absorption efficiency in the experiments performed could be found to fit within the range of 40–60%.

Further studies would be required to determine how these effects (certainly important from the laser fusion point of view) could be avoided or at least substantially suppressed by better choice of parameters of the double targets (distance between the disk and the massive target, disk diameter, its thickness and the like).

### 3.2. Crater formation by 3rd harmonic of laser radiation

To establish the wavelength influence on the efficiency of macroparticles acceleration and crater creation process, investigations employing the third harmonic of laser radiation were performed [15–17]. Targets were irradiated by the iodine laser beam:

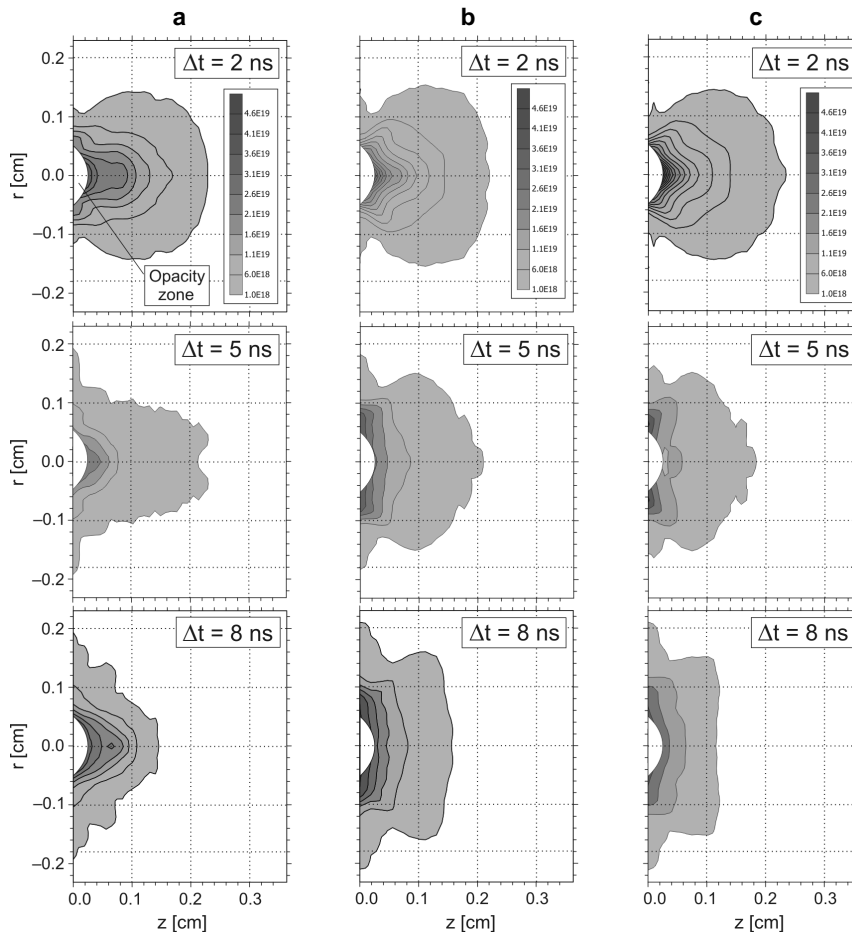


Fig. 12. Sequences of the electron density isodensitygrams for the third harmonic of the laser radiation and the three types of targets: **a** – single massive target, **b** – double target with foil, and **c** – double target with disk.

$E_L = 130$  J for the focal spot radius of  $125\ \mu\text{m}$  and the pulse duration of  $400$  ps. This laser energy was determined by the third harmonic laser energy limit and corresponded to the lowest laser energy in the former experiment. Due to the disadvantageous differences between the crater volumes for the foil and the disk with the thickness of  $11\ \mu\text{m}$  (see Fig. 10), our further investigations were performed with the macroparticle thickness of  $6\ \mu\text{m}$ . The double targets consisting of  $6\ \mu\text{m}$  thick Al foils or disks placed at the distances of  $200$  and  $500\ \mu\text{m}$  from the solid target were used. To be able to compare experimental results for the both harmonics, some additional measurements for the first harmonic of laser radiation (at the same experimental conditions) were also performed.

Typical sequences of interferograms, obtained by means of the 3-frame interferometer and showing the ablative plasma expansion and the foil motion in case of the first harmonic, are presented in Fig. 5. Multi-frame interferometric measurements of the Al foil motion provide the initial average velocity of macroparticles for the first harmonic to be equal to  $(6 \pm 0.2) 10^6$  cm/s. In the case of the third harmonic (under the same irradiation conditions) this velocity is about 2.5 times higher than that for the first harmonic.

The typical sequences of electron density distributions in a form of isodensitograms at different moments of plasma expansion for all tested target types irradiated by the first and the third harmonic are presented in Figs. 11 and 12, respectively.

The plasma stream boundary is represented by the electron density contour  $n_e = 1 \times 10^{18}$  cm<sup>-3</sup>. All subsequent equidensity lines are always separated by the value  $\Delta n_e = 5 \times 10^{18}$  cm<sup>-3</sup>.

On the basis of these interferometric measurements we could come to the following conclusions.

### 3.2.1. First harmonic

At  $\Delta t = 2$  ns the  $n_e(r, z)$  distributions are nearly identical for all three types of targets. Some major differences are becoming apparent only at later times ( $\Delta t = 8$  ns) and they particularly concern: i) the extension of the low density plasma clouds, ii) the growth of  $n_e$  in the vicinity of the massive target.

### 3.2.2. Third harmonic

Differences in  $n_e(r, z)$  for different types of targets are becoming apparent already at the very early times of  $2$  ns. While the outer shapes of plasma streams are similar in all cases, forms of the dense plasma outflows for the single massive target and the double targets differ considerably. In the case of single massive target this outflow is concentrated along the axis of symmetry whereas in the cases of double targets the axial plasma stream is shorter and exhibits plasma rings located close to the massive target surface (seen in the form of *wings* in the electron density distributions). In the subsequent period the differences between the single target and the double targets grow and concern both the low density plasma (*i.e.*, the size and shape of the plasma stream) as well as the dense plasma, represented by the inner equidensity lines.

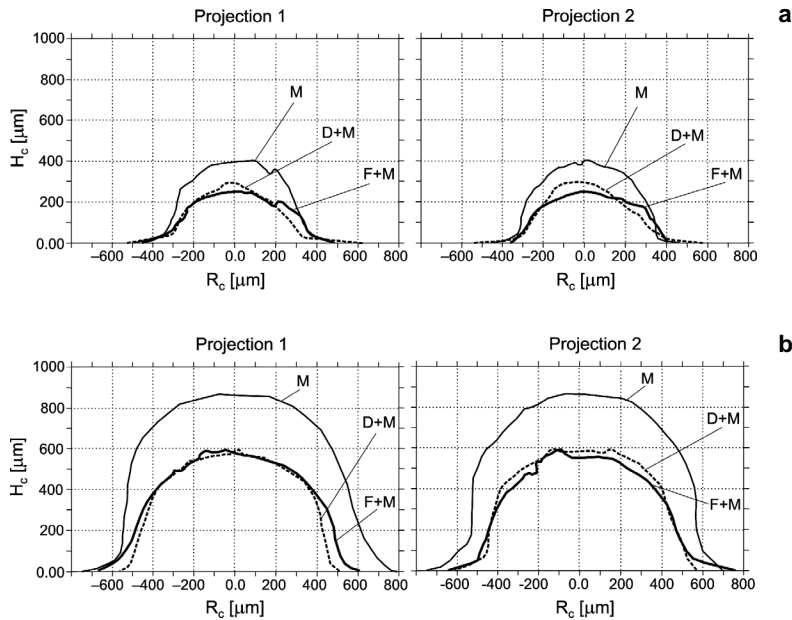


Fig. 13. Craters shapes and dimensions for the first (a) and the third (b) harmonic of the laser radiation: M – single massive target, F+M – double target with foil, and D+M – double target with disk.

The shapes of the craters and the craters dimensions for the cases of both harmonics of the laser radiation are shown in Fig. 13 ( $R_c$  and  $H_c$  denote the radius and the depth of the craters, respectively).

Based on these shapes, the following conclusions could be deduced: i) the craters created as a result of the direct laser beam-massive target interaction acquire approximately hemispherical shapes, ii) in the case of double targets the craters' shapes are similar to each other, but for the first harmonic the craters are shallower and less symmetrical, whereas for the third harmonic the craters shapes are close to hemispherical ones.

The essential difference between the first and the third harmonic cases concerns the craters volumes. The volumes of the craters shown in Fig. 13 are summarized in Tab. 2. This table clearly shows that for the same harmonics, the differences of the craters volumes between the two types of double targets are relatively small, whereas much more noticeable differences between the craters volumes are observed in case of different harmonics. For the massive targets, the craters volumes created by the third

Table 2. Set of average crater volumes for all three target types and both wavelengths (in  $\text{cm}^3$ ).

	Single massive target	Double target	
		With foil	With disk
$1\omega$	$1.03 \times 10^{-4}$	$0.64 \times 10^{-4}$	$0.62 \times 10^{-4}$
$3\omega$	$7.46 \times 10^{-4}$	$3.31 \times 10^{-4}$	$3.05 \times 10^{-4}$

harmonic are about 7.2 times larger than those created by the first harmonic. In the case of the double targets, the craters' volumes for the third harmonic are about 5 times larger than those for the first harmonic. Craters creation efficiencies in the case of the foil fragments and the disks in comparison with the craters creation efficiencies in the case of the direct laser beam action on the massive target amount to 60% and 40–45% for the first and the third harmonic, respectively.

### 3.2.3. Comparison of $1\omega$ and $3\omega$ experiments

Differences in the  $n_e(r, z)$  distributions related to the first and the third harmonic are connected with some properties of the PALS iodine laser beam. In the case of the output laser energy below 180 J the intensity distribution is approximately flat over its entire cross section. For higher output laser energies, however, the laser light amplification process causes an intensity decrease on the axis of symmetry, the depth of which increases with increasing laser energy. The 180 J threshold concerns only the first harmonic of the laser radiation. To get any required laser energy on the target in the case of the third harmonic, the output laser energy (on the first harmonic) needs to be 2–3 times larger (mainly due to the wavelength conversion efficiency – typically in the range of 30–50%). The concave character of the intensity distribution is even more pronounced in the case of the third harmonic due to the nonlinear conversion efficiency of the DKDP crystal.

Similarity of the character of the plasma expansion for all the tested targets in the case of the first harmonic is connected with the flat intensity distribution of the laser radiation. This homogeneous irradiation of the double targets preserves the flat form of the foil (and disk) and the plasma expansion can be realized analogously to that for the single massive target. In the case of the third harmonic, however, the outer forms of the plasma streams for all three target types are rather similar. One can assume that the initial conditions of the plasma emission were similar, too. However, differences concern the inner dense plasma region which appears a bit later. The elongated shape of this dense plasma in the case of the massive target is typical of the annular irradiation of the flat target [15]. Even if the irradiation conditions for the both types of double targets were the same as in the case of the massive target alone, the shape of the dense plasma noticeably differs. This difference can only be explained by the foil/disk target deformation during the laser action. This deformation should have a ring-like form, in accordance with the laser beam radiation intensity distribution. Reconstruction of plasma emission from such deformed target surface is in a good agreement with the actual electron density distribution. The growth of the electron density in the vicinity of the single massive target at the time of 8 ns after the laser action for the both harmonics can testify to a new plasma source appearance. This source can only be connected with the crater creation. At this time the accelerated macroparticles already run far away from their initial positions. Therefore, in the case of double targets such subsequent increase in plasma density does not appear.

Our initial expectation concerning possible higher efficiency of the crater creation by the accelerated disk, in comparison with the foil fragment (when some part of the

laser energy goes on the fragment extraction) has not materialized. Presented images of foil acceleration (see Fig. 7) show that there is no extraction of the foil fragment, but the great foil area, much more than the laser spot area, is accelerated. So, energy losses during the foil acceleration may be connected with damping of a foil motion by the non-irradiated part of the foil.

One important conclusion can be drawn from the comparison of crater volumes in the case of the double targets. The efficiency of the energy transfer during the non-elastic impact of the accelerated macroparticle with the wall at rest  $\beta$  (*i.e.*, the fraction of the macroparticle energy transferred to the wall) depends on the relation between the densities of the macroparticle  $\rho_p$  and the wall  $\rho_w$  as well as the adiabatic indices of both materials. According to the calculations [18], for the same densities of colliding elements ( $\rho_p = \rho_w$ ) and the adiabatic index  $\gamma_s = 5/2$  (for Al), the efficiency of the macroparticle energy transfer  $\beta = 0.58$ . For the first harmonic this value is in a good agreement with the experimental value of the relative efficiency of the crater creation by means of the macroparticles with respect to that in the case of direct laser beam action (about 60%). This agreement of the theoretical and experimental results testifies that both the foil fragment and the disk conserve their compact form and initial Al density until their collision with the massive part of the target. In case of the third harmonic the above mentioned relative efficiency of the crater creation was found equal to 0.4–0.45. This lower efficiency allows us to expect that in this case macroparticles undergo decomposition during their flight and they have impact density smaller than the value of the initial Al solid state density. The considerably lower relative efficiency of the energy transfer to the massive part of the target at the impact in the case of the third harmonic results from the much larger energy of the shock wave propagating in the macroparticles in comparison with the case of the first harmonic. It is in agreement with the experimental results for the massive targets and the theoretical prediction of a strong growth of the ablation loading efficiency (defined as the ratio of the shock wave energy to the absorbed laser energy) with a decreasing laser radiation wavelength. Indeed, when the laser radiation of the third harmonic acts, the shock wave energy and, in consequence, the temperature of the macroparticles (both foils and disks) are several times higher than those for the first harmonic. Therefore decomposition of the macroparticles before impact in the case of the third harmonic runs considerably faster.

#### 4. Numerical modelling of the crater formation process

The numerical modelling was performed by means of 2-D Lagrangian hydrodynamics code (ATLANT-HE) [19]. This code is based on one-fluid and two-temperatures model of plasma with electron and ion heat conductivity consideration. It includes laser radiation reflection, inverse bremsstrahlung and resonant absorption, as well as fast electron generation and transport.

The calculations were carried out for the first and third harmonic of laser irradiation for the following target irradiation conditions: laser energy of 130 J, laser pulse

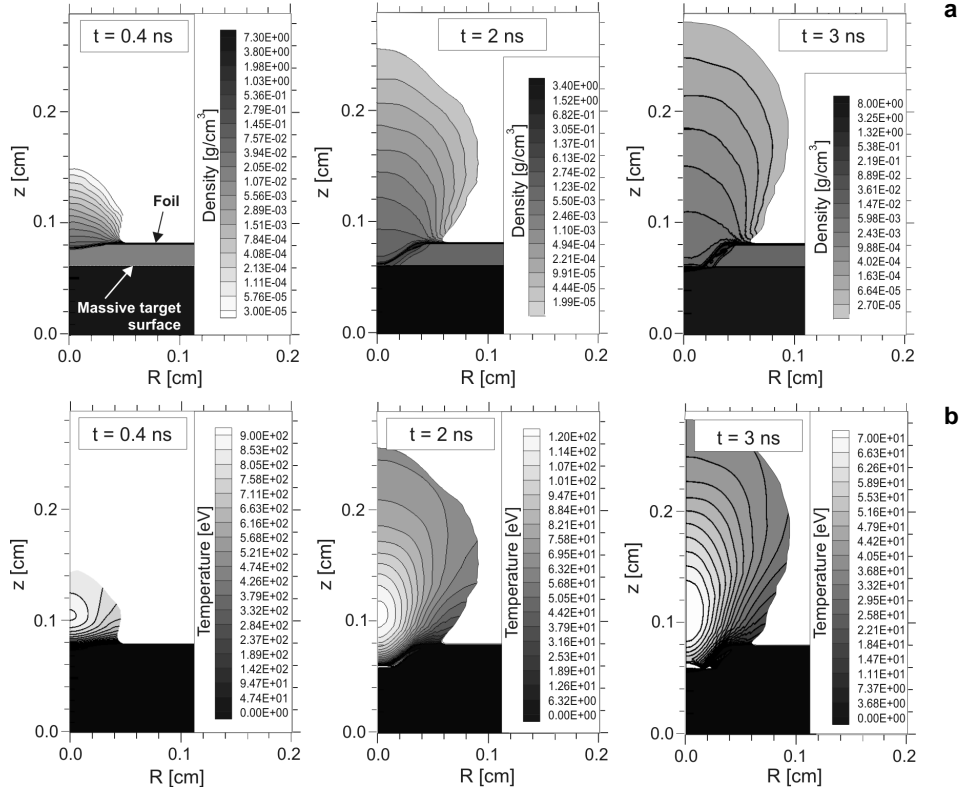


Fig. 14. Simulation of the ablative plasma generation and the foil acceleration: **a** – density and **b** – temperature.

duration of 400 ps and the focal spot radius of 125  $\mu\text{m}$ . The double target consisted of the foil with a thickness of 6  $\mu\text{m}$  separated from the massive part of the target by 200  $\mu\text{m}$ . The results of numerical calculation correspond reasonably well to the experimental data.

In the case of double targets, the processes induced by the laser beam action can be separated into two stages: i) foil fragment acceleration due to the ablation pressure and ii) crater formation as a result of the collision of the accelerated foil fragment with the massive target. Numerical modelling of the process of the foil acceleration in the case of the first harmonic is depicted in Fig. 14.

The sequence of the images shows the ablative plasma stream and the foil motion in the direction opposite to the plasma expansion. The central part of the accelerated foil reaches the massive wall after 2.3 ns. In the case of the third harmonic this time is shorter than 1 ns.

Comparison of the axial velocity changes of the accelerated foil fragment as a function of time for both wavelengths is presented in Fig. 15.

It should be emphasized that the calculated ratio of maximum values for the third and the first harmonic is approximately equal to 2.5 thus well corresponding to the

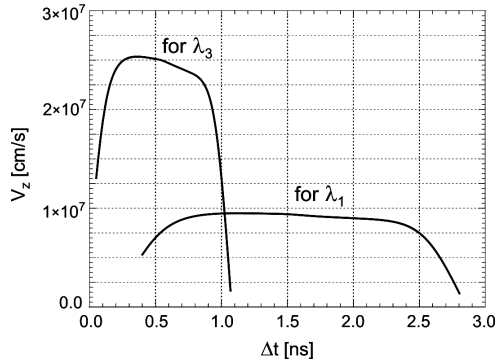


Fig. 15. Axial velocity of accelerated Al foil (at  $r = 0$ ) for both harmonics of laser radiation.

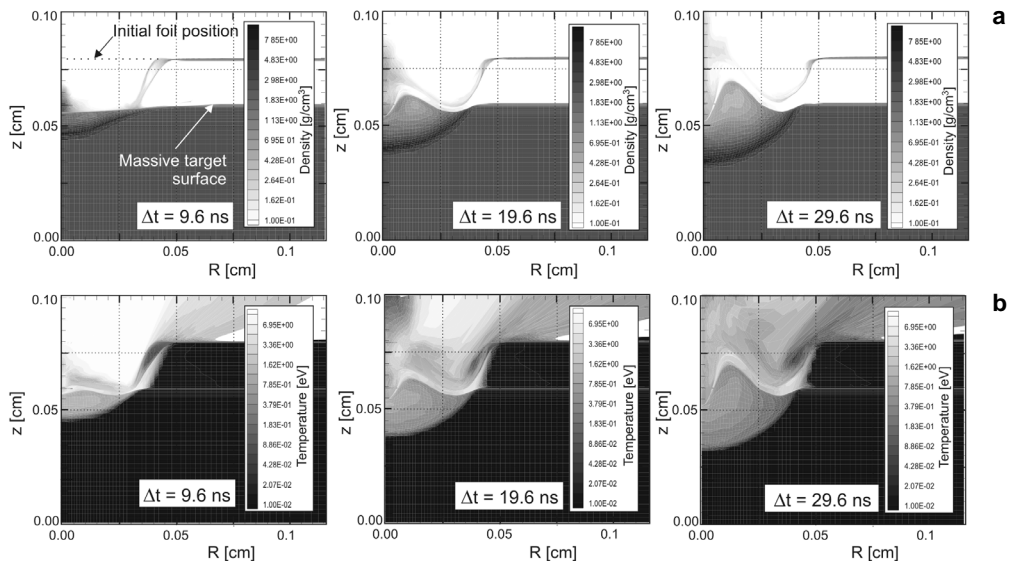


Fig. 16. Numerical modelling of the crater formation by the foil fragment impact: **a** – density and **b** – temperature.

ratio obtained from experiments. It becomes obvious that higher kinetic energy transferred into the massive target in the case of the third harmonic corresponds to higher dynamics of induced reactions.

The numerical modelling of the crater formation stage in the case of the first harmonic is presented in Fig. 16. This stage begins when the macroparticle is already completely decomposed. For the crater contour determination we used a simple procedure. If the ion temperature behind the shock wave front was higher than  $T_{cr} = 0.4$  eV (the critical temperature in Van der Waals equation of state) the contour moves together with the shock wave front. When the ion temperature becomes less than  $T_{cr}$  the contour position was fixed (no more melting).

T a b l e. 3. Energy absorption balance of the incident laser energy for the two wavelengths (all values in %).

	Inverse bremsstrahlung absorption	Resonance absorption	Efficiency of energy transfer into fast electrons
1st harmonic	47	2.1	1.8
3rd harmonic	97	2.2	0

The crater parameters obtained numerically by means of the above mentioned procedure differ from the experimental ones. The main difference concerns the crater depth, *i.e.*, the crater depths obtained numerically are about 25% smaller than the values measured in the experiment.

Numerical calculations allowed us to obtain the energy absorption balance of the incident laser energy for both wavelengths employed which is presented in Tab. 3. These data show that in the case of the third harmonic the laser energy absorption is almost full, whereas in the case of the first harmonic only about 50% of the laser energy is absorbed. The inverse bremsstrahlung absorption mechanism is dominating in both cases. Thus, the efficiency of energy transfer into fast electrons is very small.

The efficiency  $\beta$  obtained from this calculation is higher than the experimental one and amounts to 0.77. This discrepancy could be attributed to a simple model of the phase transition as well as to the use of rather simplified equation of state (perfect gas).

Although the results of the numerical modelling give a suitable qualitative picture of the investigated phenomena, some quantitative aspects of our computations should be improved.

## 5. Conclusions

The PALS iodine laser facility is a very attractive tool for investigations of ICF problems. However an access to this laser facility is very limited. That is why our experimental investigations concern only a few cases of interest. On the other hand, such great experimental arrangement creates many unexpected technical problems, so the achieved experiences will be very helpful during our subsequent investigations.

Experimental investigations performed confirmed a very useful role of the interferometric method for visualization of the laser-produced plasma expansion and determination of the dynamics of the plasma and the accelerated macroparticles. This active plasma diagnostic method, although rather complex (both technically and methodologically), is irreplaceable in such experiments.

On the other hand, the relatively simple replica method of the crater parameters measurement also delivers many interesting and important information about interaction of the laser beam or macroparticles with the massive target. Both these methods give evidence about the processes of laser energy transformation into the energy of the shock wave in solids, of the energy transfer from the laser-driven

accelerated macroparticle to the massive target, and even the absorption efficiency of the laser radiation in plasmas.

Complementary 2-D numerical simulations using hydrodynamic code are under development. At present they can provide the qualitative picture of the processes under observation and thus to help interpret the experimental data. Some quantitative aspects of these computations still need to be improved.

*Acknowledgements* – The work was supported in part by the “Access” EU program (contract HPRI-CT-1999-0053), by the Russian Foundation of Basic Research (Project 02-02-16966), IAEA (Research Project 11655/RBF), and INTAS (Project 01-0572). Czech participation was also supported by MSMT CR (Project LN00A100), PALS operational cost by AS CR (Grant K2043105).

## References

- [1] EIDMANN K., AMIRANOFF F., FEDOSEJEVS R., MAASWINKEL A.G.M., PETSCH R., SIGEL R., SPINDLER G., TENG YUNG-LU, TSAKIRIS G., WITKOWSKI S., *Interaction of 1.3- $\mu\text{m}$  laser radiation with thin foil targets*, Physical Review A: General Physics **30**(5), 1984, pp. 2568–89.
- [2] GRUN J., OBENSCHAIN S.P., RIPIN B.H., WHITLOCK R.R., MCLEAN E.A., GARDNER J., HERBST M.J., STAMPER J.A., *Ablative acceleration of planar targets to high velocities*, Physics of Fluids **26**(2), 1983, pp. 588–97.
- [3] RIPIN B.H., DECOSTE R., OBENSCHAIN S.P., BODNER S.E., MCLEAN E.A., YOUNG F.C., WHITLOCK R.R., ARMSTRONG C.M., GRUN J., STAMPER J.A., GOLD S.H., NAGEL D.J., LEHMBERG R.H., MCMAHON J.M., *Laser-plasma interaction and ablative acceleration of thin foils at  $10^{12}$ – $10^{15}$  W/cm<sup>2</sup>*, Physics of Fluids **23**(5), 1980, pp. 1012–30.
- [4] PISARCZYK T., BORODZIUK S., KASPERCZUK A., JUNGWIRTH K., KRALIKOVA B., KROUSKY E., MASEK K., PFEIFER M., ROHLENA K., SKALA J., ULLSCHMIED J., KALAL M., LIMPOUCH J., PISARCZYK P., *Application of the laser simulation method of crater creation in the laser-Al solid target experiment on the PALS facility*, Journal of High Temperature Material Processes **7**(3), 2003, pp. 319–26.
- [5] BORODZIUK S., KASPERCZUK A., PISARCZYK T., ROHLENA K., ULLSCHMIED J., KALAL M., LIMPOUCH J., PISARCZYK P., *Application of laser simulation method for the analysis of crater formation experiment on PALS laser*, Czechoslovak Journal of Physics **53**(9), 2003, pp. 799–810.
- [6] DOSKACH I., GUS'KOV S., JUNGWIRTH K., KALAL M., KASPERCZUK A., KRALIKOVA B., KROUSKY E., LIMPOUCH J., MASEK K., PFEIFER M., PISARCZYK T., ROHLENA K., ROZANOV V., SKALA J., ULLSCHMIED J., *Laser-produced post-pulse crater formation in solids observed in PALS facility interaction experiment*, Proceedings of SPIE **5228**, 2003, pp. 121–30.
- [7] JUNGWIRTH K., CEJNAROVA A., JUHA L., KRALIKOVA B., KRASA J., KROUSKY E., KRUPICKOVA P., LASKA L., MASEK K., MOCEK T., PFEIFER M., PRAG A., RENNEN O., ROHLENA K., RUS B., SKALA J., STRAKA P., ULLSCHMIED J., *The Prague Asterix Laser System PALS*, Physics of Plasmas **8**(5), 2001, pp. 2495–501.
- [8] KASPERCZUK A., PISARCZYK T., *Application of automated interferometric system for investigation of the behaviour of a laser-produced plasma in strong external magnetic field*, Optica Applicata **31**(3), 2001, pp. 571–97.
- [9] KASPERCZUK A., MAKOWSKI J., PADUCH M., TOMASZEWSKI K., WERESZCZYNSKI Z., WOLOWSKI J., WYZGAL J., *Application of fast three-frame interferometry to investigation of laser plasma*, J. Proceedings of SPIE **2202**, 1993, pp. 449–52.
- [10] PISARCZYK T., RUPASOV A.A., SARKISOV G.S., SHIKANOV A.S., *Faraday rotation method for magnetic field diagnostic in a laser plasma*, Journal of Soviet Laser Research **11**(1), 1990, pp. 1–32.
- [11] KALAL M., NUGENT K.A., *Abel inversion using fast Fourier transforms*, Applied Optics **27**(10), 1988, pp. 1956–9.

- [12] GUS'KOV S.YU., BORODZIUK S., KASPERCZUK A., PISARCZYK T., KALAL M., KRALIKOVA B., KROUSKY E., LIMPOUCH J., MASEK K., PFEIFER M., ROHLENA K., SKALA J., ULLSCHMIED J., PISARCZYK P., *Shock wave generation and crater formation in solids by a short laser pulse interaction*, Quantum Electronics **34**(11), 2004, pp. 989–1003.
- [13] BORODZIUK S., DOSKACH Y. A., GUS'KOV S.YU., JUNGWIRTH K., KALAL M., KASPERCZUK A., KRALIKOVA B., KROUSKY E., LIMPOUCH J., MASEK K., PFEIFER M., PISARCZYK P., PISARCZYK T., ROHLENA K., ROZANOV V.B., SKALA J., ULLSCHMIED J., *Experimental and theoretical investigations of craters formation in an aluminum target in a PALS experiment*, Nukleonika **49**(1), 2004, pp. 7–14.
- [14] PISARCZYK T., BORODZIUK S., KASPERCZUK A., DEMCHENKO N.N., GUS'KOV S.YU., ROZANOV V.B., KALAL M., LIMPOUCH J., JUNGWIRTH K., KRALIKOVA B., KROUSKY E., MASEK K., PFEIFER M., ROHLENA K., SKALA J., ULLSCHMIED J., KONDRASHOV V.N., PISARCZYK P., *Experimental and theoretical studies of the crater formation process on PALS experiments*, Czechoslovak Journal of Physics **54**(C), 2004, pp. 403–8.
- [15] BORODZIUK S., KASPERCZUK A., PISARCZYK T., GUS'KOV S.YU., ULLSCHMIED J., KRALIKOVA B., ROHLENA K., SKALA J., KALAL M., PISARCZYK P., *Investigation of plasma ablation and crater formation processes in the Prague Asterix Laser System laser facility*, Optica Applicata **34**(1), 2004, pp. 31–42.
- [16] KALAL M., LIMPOUCH J., BORODZIUK S., KASPERCZUK A., PISARCZYK T., DEMCHENKO N.N., GUS'KOV S.YU., ROZANOV V.B., ROHLENA K., SKALA J., ULLSCHMIED J., KONDRASHOV V.N., PISARCZYK P., *Investigation of the wavelength influence of the efficiency of macroparticles acceleration an craters creation in the PALS double targets experiment*, Czechoslovak Journal of Physics **54**(C), 2004, pp. 415–20.
- [17] BORODZIUK S., KASPERCZUK A., PISARCZYK T., DEMCHENKO N.N., GUS'KOV S.YU., ROZANOV V.B., KALAL M., LIMPOUCH J., ULLSCHMIED J., KONDRASHOV V.N., PISARCZYK P., *Application of the 3-frame interferometry and the crater replica method for investigation of laser accelerated macroparticles interacting with massive targets in the PALS experiment*, Optica Applicata **34**(3), 2004, pp. 385–403.
- [18] GUS'KOV S.YU., *Direct ignition by the drivers of different types*, Proceedings of SPIE **5228**, 2003, pp. 221–32.
- [19] ISKAKOV A.B., DEMCHENKO N.N., LEBO I.G., ROZANOV V.B., TISHKIN V.F., *2D Lagrangian code "ATLANT-HE" for simulation of plasma interaction with allowance for hot electron generation and transport*, Proceedings of SPIE **5228**, 2003, pp. 143–50.

*Received December 20, 2004*